

# Ink-Jet Printable, Self-Assembled, and Chemically Crosslinked Ion-Gel as Electrolyte for Thin Film, Printable Transistors

Jaehoon Jeong, Gabriel Cadilha Marques, Xiaowei Feng, Dominic Boll, Surya Abhishek Singaraju, Jasmin Aghassi-Hagmann, Horst Hahn,\* and Ben Breitung\*

Electrolyte-gated transistors (EGTs) represent an interesting alternative to conventional dielectric-gating to reduce the required high supply voltage for printed electronic applications. Here, a type of ink-jet printable ion-gel is introduced and optimized to fabricate a chemically crosslinked ion-gel by self-assembled gelation, without additional crosslinking processes, e.g., UV-curing. For the self-assembled gelation, poly(vinyl alcohol) and poly(ethylene-*alt*-maleic anhydride) are used as the polymer backbone and chemical crosslinker, respectively, and 1-ethyl-3-methylimidazolium trifluoromethanesulfonate ([EMIM][OTf]) is utilized as an ionic species to ensure ionic conductivity. The as-synthesized ion-gel exhibits an ionic conductivity of  $\approx 5 \text{ mS cm}^{-1}$  and an effective capacitance of  $5.4 \mu\text{F cm}^{-2}$  at 1 Hz. The ion-gel is successfully employed in EGTs with an indium oxide ( $\text{In}_2\text{O}_3$ ) channel, which shows on/off-ratios of up to  $1.3 \times 10^6$  and a subthreshold swing of  $80.62 \text{ mV dec}^{-1}$ .

voltages for operation<sup>[1–7]</sup> and remarkable progress has been made in the development of semiconducting channel materials<sup>[8–11]</sup> and gate insulators.<sup>[12–14]</sup> The EGTs are switched on/off by applying a gate potential, which leads to a migration and local redistribution of ions at the semiconductor/electrolyte interfaces. The formed electric double layer (EDL) generates high charge accumulation in the adjacent semiconducting channel, which, for instance, renders the channel conductive at a certain gate potential. For this reason, it is important for gate insulators to show high ionic conductivities, in order to quickly develop strong EDLs that improve the EGT performance. However, the switching speed of EGTs, which is slower than that for dielectric gating, is

still considered as a technical hurdle for practical applications. Therefore, various types of advanced polymer electrolytes have been intensively studied.


A different approach has been established in the last few years, where an ion-gel, consisting of an ionic liquid and a polymer, is used as a gate insulator in EGTs.<sup>[14–16]</sup> This approach makes use of the intrinsic properties of ionic liquids, such as high ionic conductivities, negligible volatility, and

## 1. Introduction

In the past years, printed electronics has been highlighted to be a very promising technique for the preparation and assembly of low power electronics, suitable for sensors and devices needed for the future development of the Internet of Things (IoT). Especially, electrolyte-gated transistors (EGTs) have been in the focus of interest, because of the possibility to use low

J. Jeong, G. C. Marques, X. Feng, D. Boll, S. A. Singaraju, Prof. J. Aghassi-Hagmann, Prof. H. Hahn, Dr. B. Breitung  
Institute of Nanotechnology (INT)  
Karlsruhe Institute of Technology (KIT)  
76344 Eggenstein-Leopoldshafen, Germany  
E-mail: horst.hahn@kit.edu; ben.breitung@kit.edu

J. Jeong, D. Boll, Prof. H. Hahn  
Joint Research Laboratory Nanomaterials - Technische Universität  
Darmstadt and Karlsruhe Institute of Technology (KIT)  
Otto-Berndt-Str. 3, 64206 Darmstadt, Germany

 The ORCID identification number(s) for the author(s) of this article can be found under <https://doi.org/10.1002/admi.201901074>.

© 2019 The Authors. Published by WILEY-VCH Verlag GmbH & Co. KGaA, Weinheim. This is an open access article under the terms of the Creative Commons Attribution-NonCommercial License, which permits use, distribution and reproduction in any medium, provided the original work is properly cited and is not used for commercial purposes.

G. C. Marques  
Chair of Dependable Nano Computing (CDNC)  
Department of Computer Science (ITEC)  
Karlsruhe Institute of Technology (KIT)  
76131 Karlsruhe, Germany

Prof. J. Aghassi-Hagmann  
Department of Electrical Engineering and Information Technology  
Offenburg University of Applied Sciences  
77652 Offenburg, Germany

Prof. H. Hahn  
Helmholtz Institute Ulm for Electrochemical Energy Storage  
Helmholtzstr. 11, 89081 Ulm, Germany

Dr. B. Breitung  
Karlsruhe Nano Micro Facility  
Karlsruhe Institute of Technology  
Hermann-von-Helmholtz-Platz 1, 76344  
Eggenstein-Leopoldshafen, Germany

DOI: 10.1002/admi.201901074

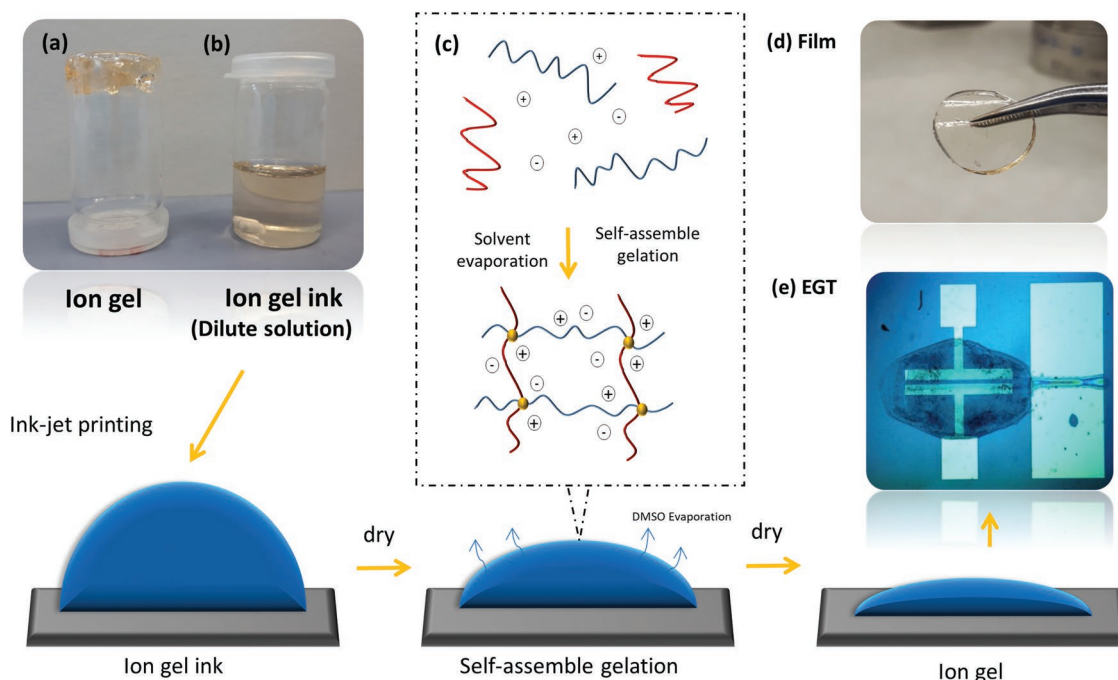


**Figure 1.** Schematic illustration of ink preparation and synthesis of PVA/PEMA ion-gel: a) ion-gel and b) ink-jet printable ion-gel ink (dilute solution). c) Illustration of self-assembled gelation of PVA, PEMA, and [EMIM][OTf] during DMSO evaporation, d) PVA/PEMA ion-gel film, and e) top-gated, ion-gel-gated thin-film transistor.

electrochemical stability, and also can derive high capacitance by forming the ELDs with ionic liquid at the interface between electrolyte and electrode.<sup>[14,16–18]</sup> In general, ion-gels are classified into chemically crosslinked (CC) or physically crosslinked (PC) ion-gels depending on the type of crosslinker. The PC ion-gels reveal a physically crosslinked structure, which usually consists of entanglement of macromolecule chains, whereas the CC ion-gel has a covalent bonded crosslinked structure. In the field of PC ion-gels, the groups of Frisbie and Lodge developed ABA triblock ion-gels, which have been considered as cutting-edge materials for printed transistors.<sup>[12–14]</sup> PC triblock ion-gels exhibit a good tailorable morphology, due to the possibility to vary block polymers and chain length, and apply to the EGTs by the aerosol-jet printer. On the other hand, CC ion-gels have been less studied compared to PC ion-gels, due to the difficulties to control the morphology and to fabricate EGTs. These difficulties arise due to the rapid formation of rigid CC ion-gel structures by irreversible gelation, which is considered as a technical hurdle for utilization in ink-jet printing processes. For these reasons, studies on CC ion-gels have almost only focused on material developments, such as finding new synthesis methods<sup>[19–21]</sup> or improving the physical properties and ionic conductivities.<sup>[22,23]</sup> Only a few reports on the practical use in printed transistors have been reported so far.

In this study, for the first time, we introduce an ink-jet printable, chemically crosslinked ion-gel for EGT applications, demonstrating remarkable ionic conductivity and capacitance values while using a straightforward synthesis method by self-assembled gelation. The synthesized ion-gel is characterized and applied in EGTs and the performance is evaluated.

## 2. Results and Discussion

The novel ion-gel ink is designed to enable ink-jet printing of chemically crosslinked ion-gels and to avoid complex synthesis processes such as annealing,<sup>[19]</sup> UV-curing,<sup>[15,21]</sup> and reversible addition-fragmentation chain transfer (RAFT) polymerization.<sup>[12–14]</sup> To ensure ink-jet printability, it is crucial to properly inhibit or promote self-assembled gelation of the ingredients, poly(vinyl alcohol) (PVA) and poly(ethylene-*alt*-maleic anhydride) (PEMA), because the functional groups of PVA and PEMA easily react even at room temperature in a concentrated solution, forming a rigid CC gel, which cannot be applied for ink-jet printing (Figure 1a).

To inhibit the self-assembled gelation and assure the ink-jet printability, our approach to effectively control the gelation is to add an excessive amount of solvent, dimethyl sulfoxide (DMSO), into the solution, which evaporates after being printed and at a certain concentration triggers the self-assembly. In dilute solution, the solvent is bound to the macromolecular coils, and these solvent-swollen coils are separated by the excess of solvent (Figure 1c).<sup>[24]</sup> For this reason, the mutual interactions are lost, and the chemical crosslinkage in the dilute solution is suppressed. When printed, the solvent evaporates slowly and the gelation of PVA and PEMA is initiated due to the release of the solvent trapped by the macromolecular coils (Figure 1d). PVA and PEMA are now able to interact mutually and to form the crosslinked CC structure directly on the substrate (Figure 1e). This self-assembled gelation does not require an additional initiation step, because the ring-opening reaction between the functional groups of PVA and PEMA is spontaneous and can easily proceed in the solution. By this simple method, we could fabricate a CC PVA/PEMA ion-gel directly on the substrate by ink-jet printing. The ion-gel ink (Figure 1a) can

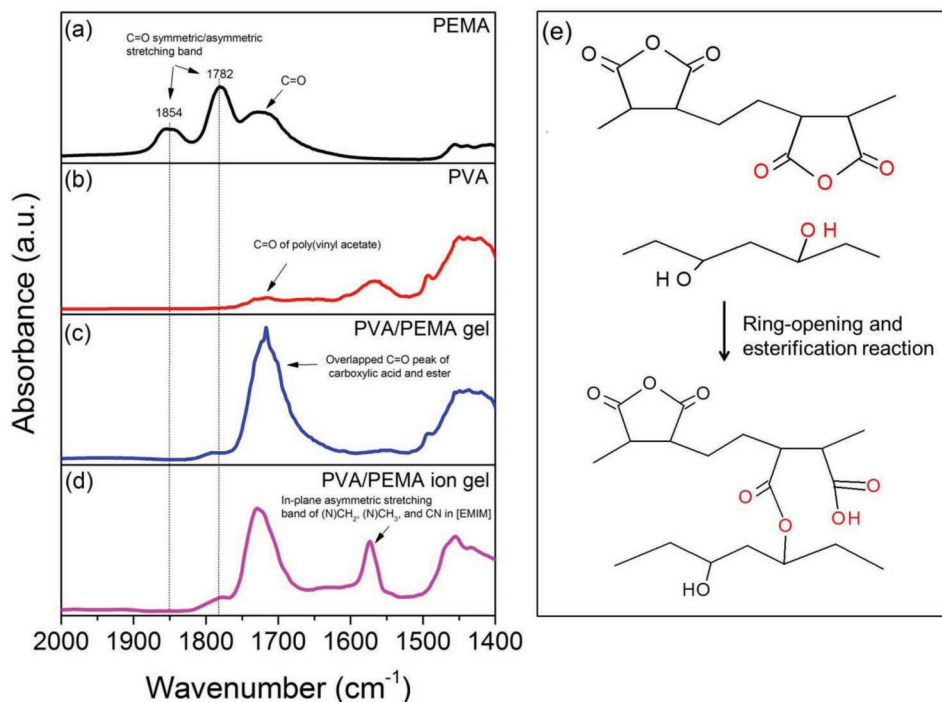


**Figure 2.** FT-IR absorbance spectrums: a) PEMA film, b) PVA film, c) PVA/PEMA polymeric gel film, and d) PVA/PEMA ion-gel film. In all cases, DMSO is fully evaporated. e) Polymer structure of PVA, PEMA, and PVA/PEMA polymeric gel.

be prepared using the following procedures: 1) separately dissolve PVA and PEMA into DMSO at 60 °C, 2) cool the temperature down to room temperature and blend PVA and PEMA solutions, 3) filter the solution with Nylon syringe filter, and 4) add [EMIM][OTf] to the solution. For a controlled inhibition of gelation, the amount of solvent was optimized.

The self-assembly of the CC structure could be tracked by Fourier-transform infrared (FT-IR) spectroscopy. In **Figure 2a** the cyclic anhydride of PEMA shows two intrinsic peaks at 1854 and 1782  $\text{cm}^{-1}$ , corresponding to C=O symmetric and asymmetric stretching bands, respectively.<sup>[25–28]</sup> The evolution of the peaks during the reaction shows that the hydroxyl (–OH) groups of PVA react with the cyclic anhydride of PEMA by a nucleophilic attack. When the solvent-swollen coils of PVA and PEMA become reactive by releasing the absorbed solvent during solvent evaporation, the cyclic anhydrides are spontaneously opened and transformed into carboxylic acid and ester groups (**Figure 2e**). The reaction can be tracked by observing the appearance of a broad peak ( $\approx 1700\text{--}1750\text{ cm}^{-1}$ ), consisting of overlapped C=O carbonyl bands of carboxylic acid (1717  $\text{cm}^{-1}$ ) and ester (1720  $\text{cm}^{-1}$ ) groups (**Figure 2c**), which can be assigned to the crosslinked structure.<sup>[28–30]</sup> Additionally, the symmetric and asymmetric C=O stretching bands (1782 and 1854  $\text{cm}^{-1}$ ), deriving from the interaction of both C=O groups of the anhydrides, disappear during the polymerization, which indicates the complete conversion of the anhydrides to carboxylic acid or ester. The additional bands in the PEMA spectrum (1700–1720  $\text{cm}^{-1}$ ) are attributed to C=O stretching bands of maleic acid which is partially hydrolyzed from maleic anhydride during the film-making process,<sup>[31]</sup> and the small peak in the PVA spectrum ( $\approx 1720\text{ cm}^{-1}$ ) is originating from

the C=O band of poly(vinyl acetate) (PVa), which is a residue in commercial PVA powder (**Figure S1**, Supporting Information).<sup>[32]</sup> When the ionic liquid is added, an additional peak appears from in-plane asymmetric stretching bands of (N)CH<sub>2</sub>, (N)CH<sub>3</sub>, and CN (1573  $\text{cm}^{-1}$ ) (**Figure 2d**).<sup>[33]</sup> Based on the FT-IR results, we assume that a chemical crosslinked structure was formed by self-assembled gelation during solvent evaporation.

The surface morphologies of PVA, PEMA, and PVA/PEMA gels were investigated using scanning electron microscopy (SEM) (**Figure 3**). The surface of PVA reveals small pores and thin thread-shaped structures on the edge of the film (**Figure 3a**), whereas PEMA shows a relatively smooth surface with some large agglomerates on the edges (**Figure 3c**). Compared to PVA and PEMA, the surface morphology of the PVA/PEMA gel is very rough, and the bundles of agglomerates are connected and stacked, creating large holes in the structure. This rough surface can be clearly observed in **Figure 3f**. We consider that these morphology differences result from the crosslinked polymer structures between PVA and PEMA.

The frequency-dependent behavior, the ionic conductivity, and the capacitance of the PVA/PEMA ion-gel are further analyzed by impedance spectroscopy in the frequency range from 100 kHz to 1 Hz. **Figure 4b** shows a log(|Z|) versus frequency plot, which depicts a plateau indicating the bulk resistance ( $R_{\text{bulk}}$ ) in the range above 30 kHz. Above this frequency, conducting ions in the ion-gel are not able to accumulate at the inner and outer Helmholtz planes (IHP and OHP) due to insufficient time for ion migration, and the EDLs cannot be formed.<sup>[34]</sup> As the frequency was decreased, the value of log(|Z|) was increased and became a tilted straight line below 3.7 kHz, corresponding to a phase angle of  $-45^\circ$ , where the polarization behavior of the EDLs

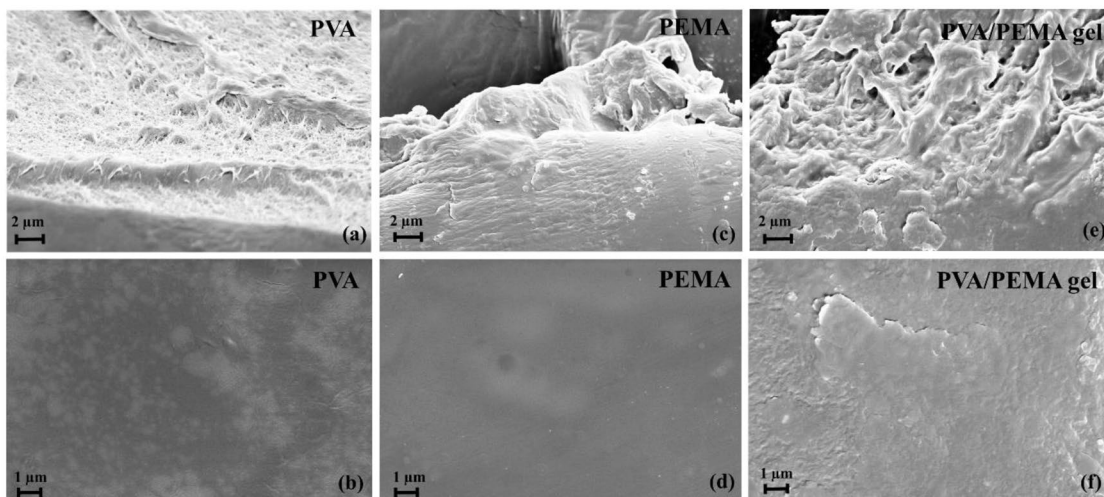


**Figure 3.** SEM micrographs of a,b) PVA, c,d) PEMA, and e,f) PVA/PEMA gel films. (a), (c), and (e) are taken at the edge of the film, and (b), (d), and (f) at the film surface. All solvent is evaporated.

is changed from resistive to capacitive.<sup>[14,35]</sup> Below 400 Hz, the phase angle was saturated between  $-70^\circ$  and  $-75^\circ$ . The deviations between a saturated phase angle and an ideal capacitive response of  $-90^\circ$  results from nonideal capacitive behavior.<sup>[34]</sup>

In addition, Figure 4c shows an ionic conductivity ( $\sigma$ ) versus frequency plot of the PVA/PEMA ion-gel. At high frequencies above 30 kHz, a plateau region of  $R_{\text{bulk}}$  is observed and the ionic conductivity is calculated to be  $\approx 5 \text{ mS cm}^{-1}$ . As the frequency is lowered, the ionic conductivity started to decrease because of electrode polarization processes by the EDLs at the electrolyte/electrode interface.<sup>[36–38]</sup> The ionic conductivity

decreases linearly below 3.7 kHz as the PVA/PEMA ion-gel exhibits capacitive behavior.

In Figure 4d, the effective capacitances ( $C_{\text{eff}}$ ) of the PVA/PEMA ion-gel were calculated using two equations, described in the literature.<sup>[16,35,39]</sup> The calculated capacitance is derived from the EDLs at the interface between ion-gel and electrode. Equation (1) is generally used to calculate the  $C_{\text{eff}}$  based on the impedance results

$$C_{\text{eff}} = \frac{-1}{2\pi fAZ_{\text{im}}} \quad (1)$$

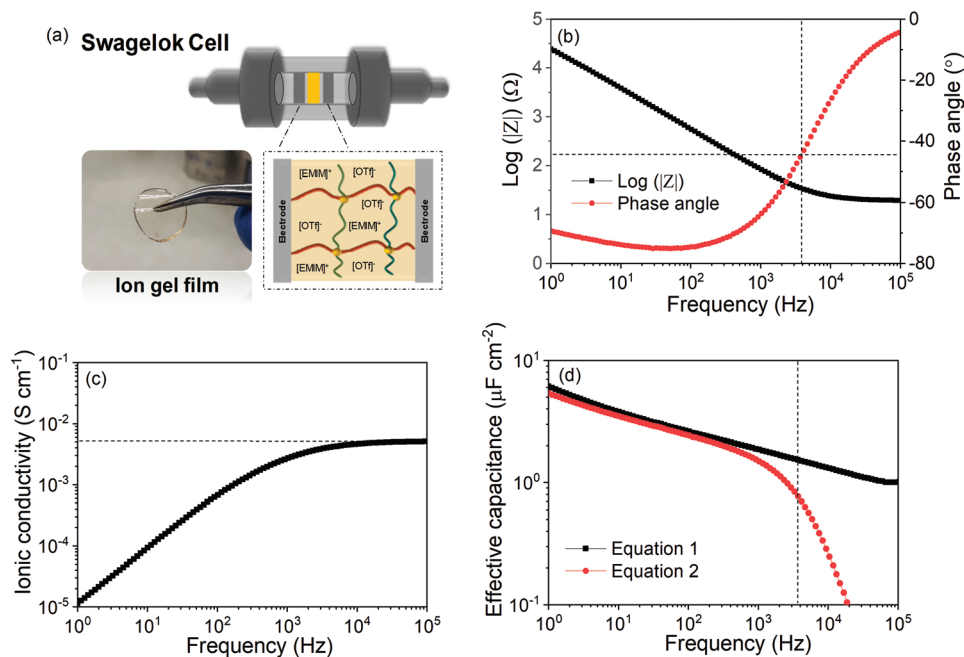


**Figure 4.** a) Illustration of a Swagelok cell assembled with two electrodes and the ion-gel film. b) Bode plot, c) ionic conductivity versus frequency plot, and d) effective capacitance ( $C_{\text{eff}}$ ) versus frequency plot of PVA/PEMA ion-gel film. Ionic conductivity and capacitance were calculated based on impedance results. The samples were measured at room temperature ( $25^\circ\text{C}$ ). Film thickness and diameter are 1.1 and 12 mm, respectively.



In Equation (1),  $f$  is the frequency,  $A$  is the surface area of electrode, and  $Z_{im}$  is the imaginary part of the impedance results. However, this equation is applicable to an ideal capacitor (phase angle ( $^\circ$ ) =  $90^\circ$ ) in the low frequency range, and deviates at high frequencies.<sup>[39–41]</sup> Figure 4b shows that the phase angle of the ion-gel is non-ideal, where the lowest phase angle (<400 Hz) is close to  $-75^\circ$ . For this reason, as suggested by Dasgupta et al.,<sup>[39]</sup> we calculated the  $C_{eff}$  using Equation (2)

$$C_{eff} = \frac{-Z_{im}}{2\pi f A |Z|^2} \quad (2)$$

In Figure 4d,  $C_{eff}$  calculated by Equation (2) is largely reduced at high frequency ranges (>3.7 kHz), where the EDLs cannot be formed and the only resistive response dominates the spectrum. Considering that the EDLs cannot be formed in the high-frequency ranges, we consider that the value for  $C_{eff}$  determined using Equation (2) is more conservative and results in values of  $5.4 \mu\text{F cm}^{-2}$  at 1 Hz.

To investigate the electric characteristics when using the PVA/PEMA ion-gel as the electrolyte, n-type top-gated EGTs with n-type indium oxide ( $\text{In}_2\text{O}_3$ ) channels were fabricated. For this purpose, indium oxide precursor is ink-jet printed between the lithographically structured drain and source electrodes (channel width and length: 600 and 20  $\mu\text{m}$ , respectively).

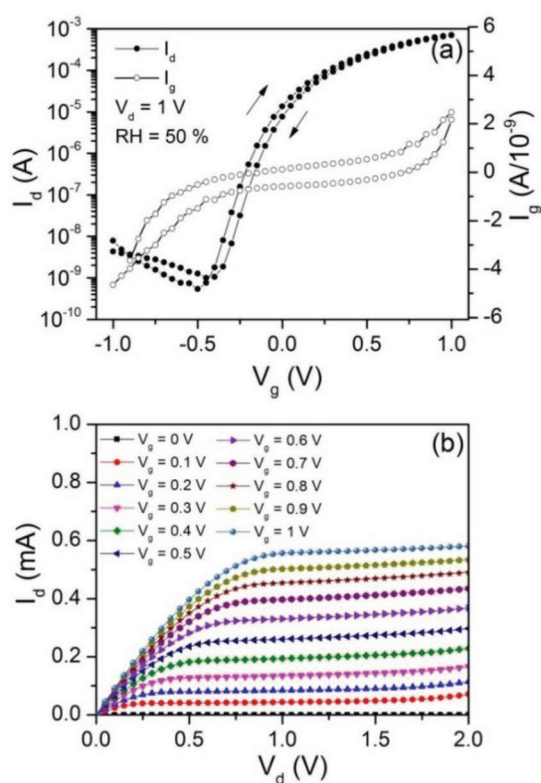


**Figure 5.** Electric characterization of top-gated EGTs: a) gate–source voltage ( $V_g$ ) versus drain–source current ( $I_d$ ) and gate current ( $I_g$ ) plots of PVA/PEMA ion-gel at 50% relative humidity (RH) and 1 V drain–source voltage ( $V_d$ ), and b)  $V_d$  versus  $I_d$  plot of PVA/PEMA ion-gel at 50% RH. Channel width and length are 600 and 20  $\mu\text{m}$ , respectively. The potential scan rate is  $0.2 \text{ V s}^{-1}$ .

After an annealing step at 400  $^\circ\text{C}$  for 2 h, the PVA/PEMA ion-gel is printed on top of the channel. After the gelation of PVA/PEMA ion-gel, poly(3,4-ethylenedioxythiophene)-poly(styrenesulfonate) (PEDOT:PSS) is printed as a top-gate electrode, covering the channel area.<sup>[4]</sup> In Figure 5a, the drain current ( $I_d$ ) and gate current ( $I_g$ ) are plotted versus the gate voltage ( $V_g$ ). The transfer curves show a narrow hysteresis and a high on/off current ( $I_{on}/I_{off}$ ) ratio of  $1.3 \times 10^6$ . The subthreshold swing (SS) obtained with the ion-gel as a gate insulator amounts to  $80.62 \text{ mV dec}^{-1}$ , which is close to the theoretical limit of  $60 \text{ mV dec}^{-1}$ . In addition, the threshold voltage ( $V_{th}$ ) is calculated to be  $-0.138 \text{ V}$  by the extrapolation of  $I_d^{1/2}$ .

In addition, the influence of humidity on PVA/PEMA ion-gel-gated transistors was tested. In previous studies, a composite solid polymer electrolyte (CSPE), consisting of PVA, propylene carbonate, and  $\text{LiClO}_4$ , has been used as a gate insulator for top-gated EGTs.<sup>[2,11,42]</sup> However, Marques et al. identified that CSPE easily loses the ionic conductivity at lower relative humidity (RH) ranges ( $\leq 20\%$ ).<sup>[43]</sup> It is assumed that trapped DMSO solvent evaporates at low humidity conditions and, as a result, the ion-transferring channels in the polymer matrix become disconnected.<sup>[43]</sup> Figure 6b shows  $I_d$  and  $I_d^{1/2}$  versus  $V_g$  plots of CSPE-gated transistors measured at 20% RH. Due to the disconnected ion channels in the polymer matrix, the CSPE loses the ionic conductivity and

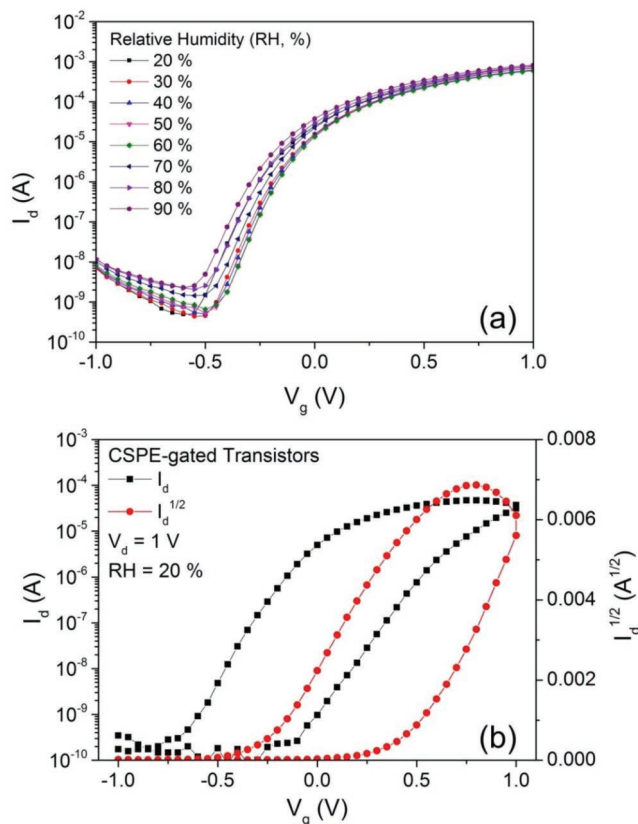


**Figure 6.** a) Gate–source voltage ( $V_g$ ) versus drain–source current ( $I_d$ ) plot of PVA/PEMA ion-gel-gated transistors at 1  $V_d$  at different relative humidities (RH, %) from 20% to 90%. b)  $V_g$  versus  $I_d$  and  $I_d^{1/2}$  plots of CSPE-gated transistors at 1  $V_d$  and 20% RH. The potential scan rate is  $0.2 \text{ V s}^{-1}$ .

**Table 1.** Electrical parameters of PVA/PEMA ion-gel-gated transistors at different values of the relative humidity (RH).

Relative humidity [%]	Off current [A]	On current [A]	On/off current ratio [ $10^5$ ]	Subthreshold swing [mV dec <sup>-1</sup> ]	Threshold voltage [V]
20	$5.01 \times 10^{-10}$	$6.86 \times 10^{-4}$	13.7	82.71	-0.241
30	$4.56 \times 10^{-10}$	$6.97 \times 10^{-4}$	15.3	80.71	-0.149
40	$5.01 \times 10^{-10}$	$6.15 \times 10^{-4}$	12.3	78.59	-0.161
50	$5.37 \times 10^{-10}$	$7.04 \times 10^{-4}$	13.1	80.62	-0.138
60	$6.55 \times 10^{-10}$	$5.89 \times 10^{-4}$	8.99	80.73	-0.154
70	$1.44 \times 10^{-9}$	$7.67 \times 10^{-4}$	5.31	85.94	-0.186
80	$2.07 \times 10^{-9}$	$7.76 \times 10^{-4}$	3.75	84.30	-0.217
90	$2.30 \times 10^{-9}$	$8.21 \times 10^{-4}$	3.58	86.01	-0.24

exhibits a clear hysteresis in the transfer curves. However, the PVA/PEMA ion-gel-gated transistors show stable transfer curves even at low RH of 20% because of the negligible volatility of [EMIM][OTf] in the polymeric gel (Figure 6a). In addition, the  $V_{th}$  and the SS parameters are stable in the range from 30% to 60% RH, whereas both parameters are increasing with humidity in CSPE-gated transistors.<sup>[43]</sup> However, at high RH levels ( $\geq 70\%$ ), the  $V_{th}$  and the SS were slightly changed in PVA/PEMA ion-gel-gated transistors. Nevertheless, this result clearly shows stable performance over all RH levels for ion-gel-gated transistors (Table 1). PEDOT:PSS was used as a top-gate electrode even though it is known that its hygroscopicity can lead to changed properties, e.g., electrical conductivity, with changing humidity.<sup>[44]</sup> However, in our results, the humidity influence has only minor impact on the transistor performance between 20% and 90% relative humidity. More drastic changes are appearing, when the relative humidity reaches values above 95%, as depicted in Figure S10 in the Supporting Information. As above, PVA/PEMA ion-gel solves the instability of CSPE against low RH level and exhibits humidity-insensitive gating performance, more suitable for practical use in room condition.

### 3. Conclusions

A new approach to synthesize chemically crosslinked ion-gels for EGTs is demonstrated in this study. The self-assembled gelation between PVA and PEMA is effectively controlled in a dilute solution and successfully adapted to the EGT fabrication by ink-jet printing. Moreover, it is determined that PVA/PEMA ion-gel shows a high ionic conductivity and effective capacitance values. In n-type top-gated EGTs, the PVA/PEMA ion-gel exhibits remarkable electrolytic properties and allows high  $I_{on}/I_{off}$  ratios, narrow hysteresis, and good SS values. Moreover, it shows humidity-insensitive performance even at low relative humidity ( $\approx 20\%$ ). This study shows new insights for the development of CC ion-gels for applications in printed electronics.

### Supporting Information

Supporting Information is available from the Wiley Online Library or from the author.

### Acknowledgements

J.J. acknowledges the German Academic Exchange Service (DAAD, Ref. No. 91650506). H.H. and J.A.H. acknowledge the funding received from Helmholtz Association under the Virtual Institute VI-530 "Printed electronics based on inorganic nanomaterials: From atoms to functional devices and circuits". S.A.S. and X.F. acknowledge the Ministry of Science, Research and Arts of the state of Baden Württemberg for funding research through the MERAGEM graduate school. B.B., J.A.S., and H.H. appreciate the support of EnABLES, a project funded by the European Union's Horizon 2020 research and innovation program under grant agreement no. 730957. Financial support by the German Research Foundation (to D.B., grant no. BR 3499/5-1) is gratefully acknowledged.

### Conflict of Interest

The authors declare no conflict of interest.

### Keywords

electrolyte-gated transistors, ink-jet print, ion-gels, ionic liquids, printed electronics

Received: June 17, 2019

Revised: July 23, 2019

Published online: September 4, 2019

- [1] S. K. Garlapati, G. C. Marques, J. S. Gebauer, S. Dehm, M. Bruns, M. Winterer, M. B. Tahoori, J. Aghassi-Hagmann, H. Hahn, S. Dasgupta, *Nanotechnology* **2018**, *29*, 235205.
- [2] F. von Seggern, I. Keskin, E. Koos, R. Kruk, H. Hahn, S. Dasgupta, *ACS Appl. Mater. Interfaces* **2016**, *8*, 31757.
- [3] S. K. Garlapati, T. T. Baby, S. Dehm, M. Hammad, V. S. K. Chakravadhanula, R. Kruk, H. Hahn, S. Dasgupta, *Small* **2015**, *11*, 3591.
- [4] G. C. Marques, S. K. Garlapati, D. Chatterjee, S. Dehm, S. Dasgupta, J. Aghassi, M. B. Tahoori, *IEEE Trans. Electron Devices* **2017**, *64*, 279.
- [5] G. C. Marques, S. K. Garlapati, S. Dehm, S. Dasgupta, H. Hahn, M. Tahoori, J. Aghassi-Hagmann, *Appl. Phys. Lett.* **2017**, *111*, 102103.
- [6] D. Weller, G. C. Marques, J. Aghassi-Hagmann, M. B. Tahoori, *IEEE Electron Device Lett.* **2018**, *39*, 831.
- [7] A. T. Erozan, G. C. Marques, M. S. Golanbari, R. Bishnoi, S. Dehm, J. Aghassi-Hagmann, M. B. Tahoori, *IEEE Trans. Very Large Scale Integr. (VLSI) Syst.* **2018**, *26*, 2935.

- [8] M. M. Alam, J. Wang, Y. Guo, S. P. Lee, H.-R. Tseng, *J. Phys. Chem. B* **2005**, *109*, 12777.
- [9] B. Nasr, D. Wang, R. Kruk, H. Rösner, H. Hahn, S. Dasgupta, *Adv. Funct. Mater.* **2013**, *23*, 1750.
- [10] T. Ozel, A. Gaur, J. A. Rogers, M. Shim, *Nano Lett.* **2005**, *5*, 905.
- [11] S. Dasgupta, R. Kruk, N. Mechau, H. Hahn, *ACS Nano* **2011**, *5*, 9628.
- [12] B. Tang, S. P. White, C. D. Frisbie, T. P. Lodge, *Macromolecules* **2015**, *48*, 4942.
- [13] Y. Gu, T. P. Lodge, *Macromolecules* **2011**, *44*, 1732.
- [14] J.-H. Choi, W. Xie, Y. Gu, C. D. Frisbie, T. P. Lodge, *ACS Appl. Mater. Interfaces* **2015**, *7*, 7294.
- [15] J.-H. Choi, Y. Gu, K. Hong, W. Xie, C. D. Frisbie, T. P. Lodge, *ACS Appl. Mater. Interfaces* **2014**, *6*, 19275.
- [16] K. H. Lee, S. Zhang, T. P. Lodge, C. D. Frisbie, *J. Phys. Chem. B* **2011**, *115*, 3315.
- [17] G. Singh, A. Kumar, *Indian J. Chem.* **2008**, *47A*, 495.
- [18] S. Murugesan, O. A. Quintero, B. P. Chou, P. Xiao, K. Park, J. W. Hall, R. A. Jones, G. Henkelman, J. B. Goodenough, K. J. Stevenson, *J. Mater. Chem. A* **2014**, *2*, 2194.
- [19] Y. Gu, S. Zhang, L. Martinetti, K. H. Lee, L. D. McIntosh, C. D. Frisbie, T. P. Lodge, *J. Am. Chem. Soc.* **2013**, *135*, 9652.
- [20] M. A. B. H. Susan, T. Kaneko, A. Noda, M. Watanabe, *J. Am. Chem. Soc.* **2005**, *127*, 4976.
- [21] G. Martínez-Ponce, C. Solano, *Opt. Express* **2006**, *14*, 3776.
- [22] M. A. Klingshirn, S. K. Spear, R. Subramanian, J. D. Holbrey, J. G. Huddleston, R. D. Rogers, *Chem. Mater.* **2004**, *16*, 3091.
- [23] K. Matsumoto, T. Endo, *Macromolecules* **2008**, *41*, 6981.
- [24] D. Braun, H. Cherdrón, M. Rehahn, G. Ritter, B. Voit, *Polymer Synthesis: Theory and Practice*, 5th ed., Springer, Berlin **2013**.
- [25] C. Q. Yang, X. Wang, *J. Appl. Polym. Sci.* **1998**, *70*, 2711.
- [26] C. Q. Yang, *J. Polym. Sci., Part A: Polym. Chem.* **1993**, *31*, 1187.
- [27] C. Q. Yang, D. Chen, J. Guan, Q. He, *Ind. Eng. Chem. Res.* **2010**, *49*, 8325.
- [28] E. Peng, E. S. G. Choo, C. S. H. Tan, X. Tang, Y. Sheng, J. Xue, *Nanoscale* **2013**, *5*, 5994.
- [29] C. Rohatgi, N. Dutta, N. Choudhury, *Nanomaterials* **2015**, *5*, 398.
- [30] W.-Y. Chiang, C.-M. Hu, *J. Appl. Polym. Sci.* **1985**, *30*, 3895.
- [31] B. Schneider, O.-D. Hennemann, W. Possart, *J. Adhes.* **2002**, *78*, 779.
- [32] D. Dibbern-Brunelli, T. D. Z. Atvars, I. Joekes, V. C. Barbosa, *J. Appl. Polym. Sci.* **1998**, *69*, 645.
- [33] N. E. Heimer, R. E. Del Sesto, Z. Meng, J. S. Wilkes, W. R. Carper, *J. Mol. Liq.* **2006**, *124*, 84.
- [34] J. Kang, J. Wen, S. H. Jayaram, A. Yu, X. Wang, *Electrochim. Acta* **2014**, *115*, 587.
- [35] O. Larsson, E. Said, M. Berggren, X. Crispin, *Adv. Funct. Mater.* **2009**, *19*, 3334.
- [36] S. Choudhary, R. J. Sengwa, *Appl. Phys.* **2011**, *49*, 10.
- [37] N. Shukla, A. K. Thakur, A. Shukla, D. T. Marx, *Int. J. Electrochem. Sci.* **2014**, *9*, 16.
- [38] Z. Osman, M. I. Mohd Ghazali, L. Othman, K. B. Md Isa, *Results Phys.* **2012**, *2*, 1.
- [39] S. Dasgupta, G. Stoesser, N. Schweikert, R. Hahn, S. Dehm, R. Kruk, H. Hahn, *Adv. Funct. Mater.* **2012**, *22*, 4909.
- [40] K. Darowicki, K. Andrearczyk, P. Slepiski, A. Sierczynska, G. Lota, K. Fic, K. Lota, *Int. J. Electrochem. Sci.* **2014**, *9*, 13.
- [41] M. Singh, K. Manoli, A. Tiwari, T. Ligonzo, C. Di Franco, N. Cioffi, G. Palazzo, G. Scamarcio, L. Torsi, *J. Mater. Chem. C* **2017**, *5*, 3509.
- [42] T. T. Baby, S. K. Garlapati, S. Dehm, M. Häming, R. Kruk, H. Hahn, S. Dasgupta, *ACS Nano* **2015**, *9*, 3075.
- [43] G. C. Marques, F. von Seggern, S. Dehm, B. Breitung, H. Hahn, S. Dasgupta, M. B. Tahoori, J. Aghassi-Hagmann, *IEEE Trans. Electron Devices* **2019**, *66*, 2202.
- [44] K. H. Choi, M. Sajid, S. Aziz, B.-S. Yang, *Sens. Actuators, A* **2015**, *228*, 40.